

## Water formation by surface O<sub>3</sub> hydrogenation

C. Romanzin,<sup>1</sup> S. Ioppolo,<sup>2</sup> H. M. Cuppen,<sup>2,3</sup> E. F. van Dishoeck,<sup>3,4</sup> and H. Linnartz<sup>2,a)</sup>

<sup>1</sup>LPMAA, Université Pierre et Marie Curie, Paris, France

<sup>2</sup>Sackler Laboratory for Astrophysics, Leiden Observatory, Leiden University, P.O. Box 9513, 2300 RA Leiden, The Netherlands

<sup>3</sup>Leiden Observatory, Leiden University, P.O. Box 9513, 2300 RA Leiden, The Netherlands

<sup>4</sup>Max-Planck-Institut für Extraterrestrische Physik, Giessenbachstrasse 1, D-85741 Garching, Germany

(Received 14 September 2010; accepted 4 December 2010; published online 24 February 2011)

Three solid state formation routes have been proposed in the past to explain the observed abundance of water in space: the hydrogenation reaction channels of atomic oxygen (O + H), molecular oxygen (O<sub>2</sub> + H), and ozone (O<sub>3</sub> + H). New data are presented here for the third scheme with a focus on the reactions O<sub>3</sub> + H, OH + H and OH + H<sub>2</sub>, which were difficult to quantify in previous studies. A comprehensive set of H/D-atom addition experiments is presented for astronomically relevant temperatures. Starting from the hydrogenation/deuteration of solid O<sub>3</sub> ice, we find experimental evidence for H<sub>2</sub>O/D<sub>2</sub>O (and H<sub>2</sub>O<sub>2</sub>/D<sub>2</sub>O<sub>2</sub>) ice formation using reflection absorption infrared spectroscopy. The temperature and H/D-atom flux dependence are studied and this provides information on the mobility of ozone within the ice and possible isotope effects in the reaction scheme. The experiments show that the O<sub>3</sub> + H channel takes place through stages that interact with the O and O<sub>2</sub> hydrogenation reaction schemes. It is also found that the reaction OH + H<sub>2</sub> (OH + H), as an intermediate step, plays a prominent (less efficient) role. The main conclusion is that solid O<sub>3</sub> hydrogenation offers a potential reaction channel for the formation of water in space. Moreover, the nondetection of solid ozone in dense molecular clouds is consistent with the astrophysical picture in which O<sub>3</sub> + H is an efficient process under interstellar conditions. © 2011 American Institute of Physics. [doi:10.1063/1.3532087]

### I. INTRODUCTION

Water is ubiquitous throughout the universe and belongs to the more abundant species in the interstellar medium. Since gas phase formation rates are not efficient at low temperatures, the formation of H<sub>2</sub>O ice in cold dense quiescent interstellar clouds (~10 K) is expected to take place in the solid state on the surface of dust grains through H-atom addition reactions. Three different hydrogenation channels have been proposed in the past: O + H, O<sub>2</sub> + H, and O<sub>3</sub> + H.<sup>1</sup> Several laboratory studies investigated the formation of solid H<sub>2</sub>O through the hydrogenation of atomic oxygen<sup>2,3</sup> and molecular oxygen.<sup>4-9</sup> However, only a single study<sup>10</sup> investigated the third channel so far, showing that the deuteration of O<sub>3</sub> ice on an amorphous H<sub>2</sub>O substrate leads to the formation of D<sub>2</sub>O by detecting HDO molecules during desorption of the ice using quadrupole mass spectrometry. We give here further experimental evidence for H<sub>2</sub>O/D<sub>2</sub>O ice formation, presenting for the first time a comprehensive set of H/D-atom addition experiments on solid O<sub>3</sub> for astronomically relevant temperatures, using reflection absorption infrared spectroscopy (RAIRS).

Solid O<sub>3</sub> can be formed in space through energetic processing (ions, photons, and electrons) of O-bearing ices at astronomically relevant temperatures.<sup>11-18</sup> Tielens and Hagen<sup>1</sup> proposed the formation of O<sub>3</sub> ice through the subsequent oxidation of atomic oxygen on the surface of the interstellar grains at low temperature and in absence of UV irradiation. Ozone ice has been observed on the surface of small bodies in the solar system, such as Ganymede, Rhea, and Dione,<sup>19-21</sup>

but it has not been observed in the interstellar medium. The nondetection of solid ozone in dense molecular clouds is consistent with an efficient use-up through hydrogenation, in the case that O<sub>3</sub> + H is an efficient process under interstellar conditions.

Figure 1, taken from Ref. 9, shows how the three hydrogenation channels (O/O<sub>2</sub>/O<sub>3</sub> + H) can interact. Specifically, the hydrogenation of solid O<sub>3</sub> comprises the following solid state reactions:



and



Cuppen and Herbst<sup>22</sup> and Cazaux *et al.*<sup>23</sup> showed in their astrochemical models that the efficiency of this reaction channel strongly depends on the astronomical environment (e.g., diffuse clouds, dense clouds, and photon-dominated regions). Ioppolo *et al.*<sup>8</sup> and Cuppen *et al.*<sup>9</sup> showed experimentally that the O + H and the O<sub>3</sub> + H channels are connected via the O<sub>2</sub> + H route through common reactive intermediates (see Fig. 1). The latter channel involves the reactions



and



<sup>a)</sup>Electronic mail: linnartz@strw.leidenuniv.nl.

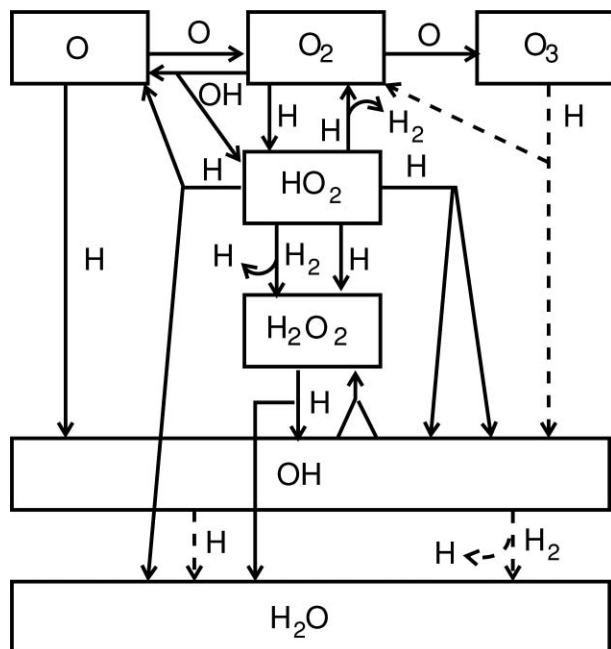


FIG. 1. A schematic representation of the water formation reaction network ( $\text{O} + \text{H}$ ,  $\text{O}_2 + \text{H}$ , and  $\text{O}_3 + \text{H}$ ). The solid arrows represent the surface reaction network as obtained from Refs. 8 and 9. The dashed arrows represent the surface reactions investigated here.

which both lead to the formation of O atoms. These can then react with  $\text{O}_2$  to form  $\text{O}_3$ ,



Indeed,  $\text{O}_3$  has been found as a reaction product in hydrogenation experiments of pure  $\text{O}_2$  ice.<sup>8,9</sup>

In the following sections, we investigate the  $\text{O}_3 + \text{H}$  scheme under interstellar analog conditions. We focus in particular on the first reaction step  $\text{O}_3 + \text{H}$  as well as the formation of  $\text{H}_2\text{O}$  from OH through reactions (2) and (3). For this purpose, most experiments are carried out at elevated temperatures in order to instantaneously desorb the  $\text{O}_2$  formed through reaction (1).

## II. EXPERIMENTAL

The experiments are performed using an ultra high vacuum set-up, which has been described in detail elsewhere.<sup>8,24</sup> It consists of an atomic beam line and a main chamber ( $\sim 10^{-10}$  mbar) in which ices are grown on a cryogenically cooled (12–300 K) gold-coated copper substrate by depositing gas under an angle of  $45^\circ$ . A fresh  $\text{O}_3$  sample is prepared before each experiment in a high-vacuum glass line, following the procedure as described in Ref. 25. The  $\text{O}_3$  sample is prepared in a commercial ozone generator (Fischer-model 502,  $\text{O}_2$  99.995% of purity, Praxair) and collected in a liquid nitrogen trap, which is used to purify the sample from  $\text{O}_2$  pollution.  $\text{O}_2$  deposition originating from the dissociation of  $\text{O}_3$  in the main chamber is kept to a minimum by maintaining the substrate temperature at 40 K, well above the  $\text{O}_2$  desorption temperature [ $T_{\text{des}}(\text{O}_2) \sim 30$  K, Ref. 26]. The ice is monitored by means of RAIRS, using a Fourier transform infrared spectrometer (FTIR). The FTIR covers the range

between 4000 and  $700\text{ cm}^{-1}$  ( $2.5\text{--}14\ \mu\text{m}$ ) with a spectral resolution of  $1\text{ cm}^{-1}$ . A coaddition of 256 scans yields one spectrum. RAIR difference spectra ( $\Delta A$ ) with respect to the deposited  $\text{O}_3$  ice spectrum are acquired every few minutes during the hydrogenation experiment. According to Sivaraman *et al.*,<sup>18</sup> shape and position of the  $\nu_3(\text{O}_3)$  stretching mode is sensitive to the ozone environment. Therefore, the presence of other molecules should affect this infrared band, but the observed  $\nu_3(\text{O}_3)$  band in our spectra after deposition is typical for a rather pure  $\text{O}_3$  ice,<sup>18,27,28</sup> instead of  $\text{O}_3$  molecules mixed with  $\text{O}_2$ .<sup>14</sup>

After deposition the ice is subsequently hydrogenated/deuterated at different temperatures (25, 40, and 50 K). H/D atoms are supplied by a well-characterized thermal cracking source.<sup>29–31</sup>  $\text{H}_2/\text{D}_2$  molecules are cracked in a capillary pipe surrounded by a tungsten filament, which is heated to 2200 K. During the H/D-atom exposure, the pressure in the atomic line is kept constant. Hot H/D atoms are cooled to room temperature via collisions by a nose-shaped quartz pipe, placed in the H/D-atom beam path toward the substrate. The geometry of the pipe is designed in such a way that hot species (H/D;  $\text{H}_2/\text{D}_2$ ) cannot reach the ice directly (more details in Refs. 8 and 24). The H/D-atom fluxes used in our experiments are set by changing the  $\text{H}_2/\text{D}_2$  pressure in the capillary pipe, while the filament temperature is kept constant. The final flux values ( $2 \times 10^{13}$  and  $8 \times 10^{13}$  atoms  $\text{cm}^{-2}\text{ s}^{-1}$  for H atoms and  $1 \times 10^{13}$  and  $4 \times 10^{13}$  atoms  $\text{cm}^{-2}\text{ s}^{-1}$  for D atoms) are measured at the substrate position in the main chamber using a quadrupole mass spectrometer for the D-atom flux. The method is described in the Appendix of Ref. 8. The relative error in the D-atom flux determination is within 10%, while the relative H-atom flux determination is within 50%. The absolute error for both is estimated to be within 50%.

Several control experiments have been carried out. Deuteration experiments have been performed to estimate the maximum  $\text{H}_2\text{O}$  contamination, i.e.,  $\text{H}_2\text{O}$  contributions other than those induced in the ice upon H-atom impact. This is essential as  $\text{H}_2\text{O}$  is the prime target of this study. The pollution may originate from  $\text{H}_2\text{O}$  background in the UHV setup and/or from  $\text{H}_2\text{O}$  in the high vacuum gas line. The contamination is found to increase with time and to be less  $\sim 1$  monolayer (ML) at the end of all experiments. Results presented in Sec. IV are corrected for this contamination. In the deuteration experiments, naturally, this contamination does not play a role. Also, a pure  $\text{O}_3$  ice has been exposed to a  $\text{D}_2$  beam (at 40 K) to ensure that the  $\text{D}_2$  molecules do not chemically react with the  $\text{O}_3$  or physically change the surface through sputtering. Finally, an unprocessed  $\text{O}_3$  ice grown at 40 K and subsequently heated to 50 K with a rate of  $1\text{ K min}^{-1}$  shows no substantial  $\text{O}_3$  loss because of thermal desorption [ $T_{\text{des}}(\text{O}_3) \sim 63$  K, Ref. 11] over a 3 h period, the length of a typical experiment.

## III. DATA ANALYSIS

After subtracting the infrared spectra with a piece-wise straight baseline, the column densities (molecules  $\text{cm}^{-2}$ ) of

TABLE I. Assigned infrared features in the 4000–700 cm<sup>-1</sup> region.

Mode	Position <sup>a</sup> (cm <sup>-1</sup> )	Species	Position <sup>a</sup> (cm <sup>-1</sup> )	Species	References
libration	830	H <sub>2</sub> O			32, 33
$\nu_3$	888	H <sub>2</sub> O <sub>2</sub>	884	D <sub>2</sub> O <sub>2</sub>	32, 34
$\nu_2, 2\nu_4, \nu_6$	1390(*)	H <sub>2</sub> O <sub>2</sub>	1050(*)	D <sub>2</sub> O <sub>2</sub>	32, 34
$\nu_2$	1650(*)	H <sub>2</sub> O	1210(*)	D <sub>2</sub> O	32, 33
$2\nu_6$	2840	H <sub>2</sub> O <sub>2</sub>	2100	D <sub>2</sub> O <sub>2</sub>	32, 34
$\nu_1, \nu_5$	3290	H <sub>2</sub> O <sub>2</sub>	2465	D <sub>2</sub> O <sub>2</sub>	32, 34
$\nu_3$	3260	H <sub>2</sub> O	2440	D <sub>2</sub> O	32, 33
$\nu_3$	1050	O <sub>3</sub>			17, 27, 35
$\nu_1$	1107	O <sub>3</sub>			17, 27, 35
$\nu_1 + \nu_3$	2110	O <sub>3</sub>			17, 27, 35

<sup>a</sup>Asterisks mark the features used to determine the integrated absorbance.

the newly formed species are calculated using the modified Lambert–Beer equation  $N_X = \int A(\nu)d\nu/S_X$ , where  $A(\nu)$  is the wavelength dependent absorbance. Since literature values of transmission band strengths cannot be used directly in reflection measurements, an apparent absorption band strength,  $S_X$  of species  $X$ , is determined by individual calibration experiments. This procedure has been described in detail elsewhere (for the H<sub>2</sub>O/D<sub>2</sub>O and H<sub>2</sub>O<sub>2</sub>/D<sub>2</sub>O<sub>2</sub> band strength determinations see Refs. 8 and 9). Briefly, a layer of the selected ice is deposited at a temperature lower than its desorption temperature. The sample is then linearly heated, close to its desorption temperature. Infrared spectra are acquired regularly until the desorption of the ice is complete. Such an isothermal desorption experiment has been performed to determine the apparent absorption band strength of O<sub>3</sub> by recording the transition from zeroth-order to first-order desorption. This is assumed to occur at the onset of the submonolayer regime and appears in the desorption curve as a sudden change in slope. The apparent absorption strength in cm<sup>-1</sup> ML<sup>-1</sup> is then calculated by relating the observed integrated area to 1 ML in the modified Lambert–Beer equation. We estimate the uncertainty of the band strength to be within 50%. The noise in the infrared spectra introduces an extra uncertainty in the H<sub>2</sub>O/D<sub>2</sub>O, H<sub>2</sub>O<sub>2</sub>/D<sub>2</sub>O<sub>2</sub>, and O<sub>3</sub> column densities, which is found to be within  $\pm 0.5$  ML for all the considered species.

The assignment of the spectral features observed in our experiments is listed in Table I. The band modes peaking at 1650/1210 cm<sup>-1</sup> ( $\nu_2$ ) and 1390/1050 cm<sup>-1</sup> ( $\nu_2, 2\nu_4, \nu_6$ ) are chosen to quantify the column densities of the newly formed species upon H/D-atom exposure (solid H<sub>2</sub>O/D<sub>2</sub>O and H<sub>2</sub>O<sub>2</sub>/D<sub>2</sub>O<sub>2</sub>, respectively). The O<sub>3</sub> band peaking at 1050 cm<sup>-1</sup> ( $\nu_3$ ) is used to quantify the amount of O<sub>3</sub> deposited on the cold substrate, and, subsequently, the O<sub>3</sub> consumed in the surface reactions during H/D-atom addition. The 1050 cm<sup>-1</sup> D<sub>2</sub>O<sub>2</sub> band overlaps with the  $\nu_3$ (O<sub>3</sub>) band in our infrared spectra. Thus, a multi-Gaussian fit is used to separate the contributions and determine the area of the individual bands.

## IV. RESULTS AND DISCUSSION

Figure 2 shows the RAIR difference spectra acquired during an hydrogenation (*left panel*) and a deuteration (*right panel*) experiment of solid O<sub>3</sub> at 25 K. Both H<sub>2</sub>O/D<sub>2</sub>O and H<sub>2</sub>O<sub>2</sub>/D<sub>2</sub>O<sub>2</sub> integrated band intensities clearly grow as the H/D-fluence (H/D-flux  $\times$  time) increases. Neither species such as OH, HO<sub>2</sub>, and HO<sub>3</sub>, nor the partially deuterated species, such as HDO and HDO<sub>2</sub>, are detected in our infrared spectra during H/D-atom addition to the O<sub>3</sub> ice. The presence of fully deuterated species gives experimental evidence for surface formation of water ice in the solid phase with O<sub>3</sub> ice as a precursor. The negative peak shown in Fig. 2 indeed reflects the O<sub>3</sub> use-up.

### A. Temperature dependence

Figure 3 shows the H<sub>2</sub>O/D<sub>2</sub>O (*square*) and H<sub>2</sub>O<sub>2</sub>/D<sub>2</sub>O<sub>2</sub> (*triangle*) column densities for the three investigated temperatures (25, 40, and 50 K) as a function of the H/D-atom fluence. The solid/open symbols correspond to the low/high H/D-atom flux used in our experiments. The amount of O<sub>3</sub> use-up (*circle*) during H/D-atom addition changes with the substrate temperature from  $\sim 1$  ML at 25 K to  $\sim 10$  ML at 50 K. This is consistent with the increase of the H/D-atom penetration depth in the O<sub>3</sub> ice at higher temperatures, since the mobility of O<sub>3</sub> molecules in the ice is expected to improve with increasing temperature, even though the penetration depth of H atoms involves only the surface of the ice and not the bulk. A similar temperature dependence has been observed for the penetration depth of H atoms in CO ice.<sup>24</sup> Another mechanism may also affect the final amount of O<sub>3</sub> use-up: the erosion of the ice. Each time an H/D atom reacts with an O<sub>3</sub> molecule through reaction (1) an O<sub>2</sub> molecule is formed. Whether the O<sub>2</sub> molecule remains on the surface of the ice

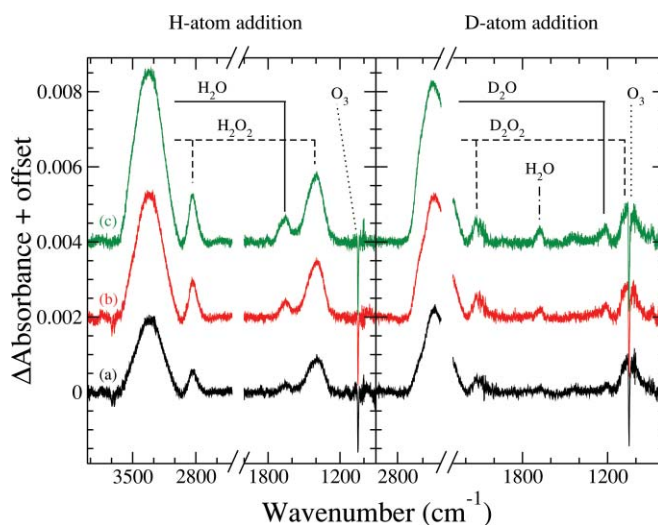


FIG. 2. Difference infrared spectra of solid O<sub>3</sub> ice, with respect to the spectrum before H/D-atom addition, upon hydrogenation/deuteration at 25 K for three different H/D-atom exposures: (a)  $2.4 \times 10^{16}$ , (b)  $7.2 \times 10^{16}$ , and (c)  $2.0 \times 10^{17}$  H/D atoms cm<sup>-2</sup> s<sup>-1</sup> (*left/right panel*, respectively). Spectra are offset for clarity. The water pollution is visible in the deuteration experiment (*right panel*).



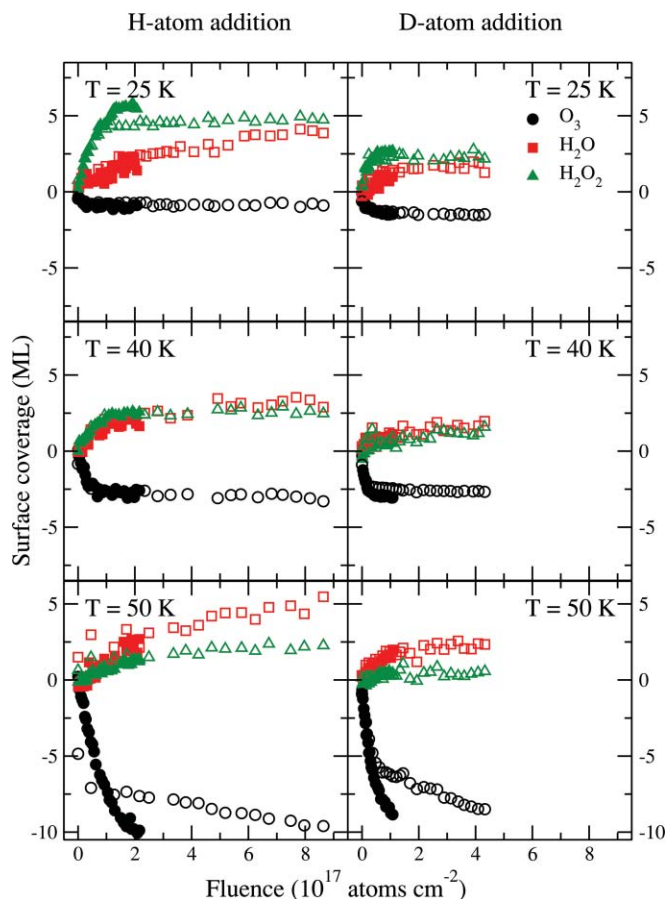


FIG. 3. Column densities for  $\text{H}_2\text{O}/\text{D}_2\text{O}$  (square),  $\text{H}_2\text{O}_2/\text{D}_2\text{O}_2$  (triangle), and  $\text{O}_3$  (circle) for the three temperatures investigated (25, 40, and 50 K) as a function of the H/D-atom fluence. The hydrogenated species are plotted in the left panel, and the deuterated species in the right panel. The solid and open symbols correspond to the lower and higher H/D-atom flux ( $2 \times 10^{13}$  and  $8 \times 10^{13}$  atoms  $\text{cm}^{-2} \text{s}^{-1}$  for H atoms and  $1 \times 10^{13}$  and  $4 \times 10^{13}$  atoms  $\text{cm}^{-2} \text{s}^{-1}$  for D atoms), respectively.

or desorbs, depends on the temperature of the ice. Below 30 K, the  $\text{O}_2$  molecules will be further hydrogenated/deuterated according to the scheme shown in Fig. 1 (see also Refs. 8 and 9). At higher temperatures (above 30 K, see Ref. 26) the desorption of the  $\text{O}_2$  formed through reaction (1) will leave the deeper  $\text{O}_3$  layers exposed for H/D-atom addition, increasing the final  $\text{O}_3$  use-up. The  $\text{H}_2\text{O}/\text{D}_2\text{O}$  and  $\text{H}_2\text{O}_2/\text{D}_2\text{O}_2$  column density ratios are also affected by this desorption behavior. Below 30 K,  $\text{H}_2\text{O}/\text{D}_2\text{O}$  will be formed through both the hydrogenation/deuteration of  $\text{O}_2$  ice and reactions (2) and (3). A significant amount of  $\text{H}_2\text{O}_2/\text{D}_2\text{O}_2$  will be formed through the  $\text{O}_2$  channel as well.<sup>8,9</sup> For increasing temperature, the  $\text{O}_2$  channel becomes less important and as a consequence the amount of  $\text{H}_2\text{O}_2/\text{D}_2\text{O}_2$  decreases, while  $\text{H}_2\text{O}/\text{D}_2\text{O}$  formation through reactions (2) and (3) becomes the dominant process.

As a side-effect of the erosion/restructuring of the ice, the  $\text{H}_2\text{O}$  pollution diluted in the  $\text{O}_3$  ice may rearrange in islands. Consequently, the narrow  $\text{H}_2\text{O}$  bands seen after deposition of the  $\text{O}_3$  ice in the region of the  $\text{H}_2\text{O}$  bending mode ( $1650 \text{ cm}^{-1}$ ) will broaden upon ice restructuring. This

effect increases with time and contributes to the total  $\text{H}_2\text{O}$  bulk feature peaking at  $1650 \text{ cm}^{-1}$ . This effect is shown in the right panel of Fig. 2. The contribution of this effect, which is estimated to be  $\sim 1 \text{ ML}$  at the end of all the deuteration experiments, is taken into account for all the H-atom addition experiments, as mentioned in Sec. II.

## B. H/D-atom flux dependence

Figure 3 also indicates the influence of the H/D-atom flux on the amount of reaction products. The  $\text{H}_2\text{O}/\text{D}_2\text{O}$  and  $\text{H}_2\text{O}_2/\text{D}_2\text{O}_2$  column densities follow the same trend for high and low H/D-atom flux and for all investigated temperatures within the experimental uncertainties. This observation is in agreement with a scenario in which a reactive system is limited only by the number of H/D atoms that reaches the ice surface. The  $\text{O}_3$  column density follows the same behavior for high and low H/D-atom flux at temperatures below 40 K and at 50 K for a maximum H/D-atom fluence of  $1 \times 10^{16}$  H/D atoms  $\text{cm}^{-2}$ . However, at higher H/D-atom fluence the  $\text{O}_3$  column density profile differs for high and low H/D-atom flux at 50 K. This is most likely caused by the transition between two different regimes: in the first regime, reaction (1) is limited by the number of H/D atoms; in the second regime, this reaction is limited by the supply of  $\text{O}_3$  molecules, since the formed  $\text{H}_2\text{O}/\text{D}_2\text{O}$  and  $\text{H}_2\text{O}_2/\text{D}_2\text{O}_2$  prevent the incoming H/D atoms to reach the  $\text{O}_3$  molecules in the lower layers. Further conversion into  $\text{H}_2\text{O}/\text{D}_2\text{O}$  and  $\text{H}_2\text{O}_2/\text{D}_2\text{O}_2$  is then only possible after replenishing of the top layers by fresh  $\text{O}_3$ . This process is governed by the diffusion of  $\text{O}_3$  in the ice, which increases with temperature and is independent of H/D-atom flux. Thus, this effect is stronger at 50 K than at 40 K and indeed the  $\text{O}_3$  use-up follows the same trend for low and high H/D-atom fluxes when plotted as a function of exposure time instead of fluence for  $> 1 \times 10^{16}$  H/D atoms  $\text{cm}^{-2}$ . The two regimes are schematically depicted in Fig. 4.

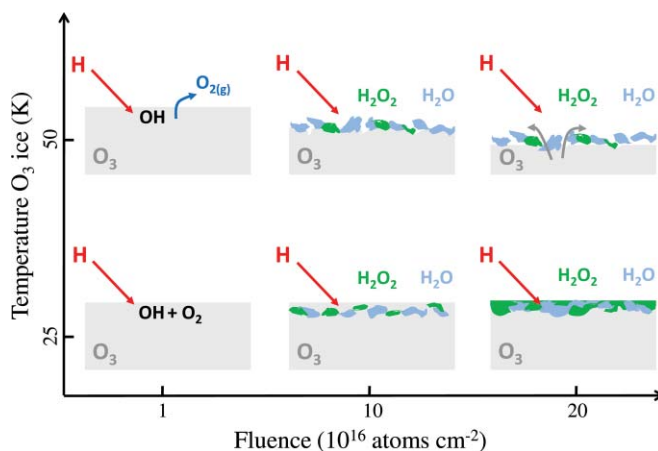


FIG. 4. Schematic representation of the hydrogenation of  $\text{O}_3$  ice as a function of the temperature and H-atom fluence: at temperatures below 40 K (bottom) reaction (1) is limited by the number of H/D atoms, at higher temperatures (top) this reaction is limited by the supply of  $\text{O}_3$  molecules. The replenishing of the top layers is induced by diffusion of  $\text{O}_3$  in the ice. The erosion of the ice at 50 K is also shown (top).

TABLE II. Amounts of O<sub>3</sub> use-up, and formed H<sub>2</sub>O/D<sub>2</sub>O and H<sub>2</sub>O<sub>2</sub>/D<sub>2</sub>O<sub>2</sub> in ML after an exposure of  $1.1 \times 10^{17}$  H/D atoms cm<sup>-2</sup> and  $4.2 \times 10^{17}$  H/D atoms cm<sup>-2</sup> (low and high fluxes, respectively) at the three different substrate temperatures investigated. See Sec. III for the determination of the values and the corresponding errors. The O<sub>budget</sub> corresponds to the mass-balance of O atoms in ML: O<sub>budget</sub> = -3O<sub>3</sub> + H<sub>2</sub>O + 2H<sub>2</sub>O<sub>2</sub>, or the equivalent for deuteration.

H/D-flux (cm <sup>-2</sup> s <sup>-1</sup> )	T (K)	O <sub>3</sub> (ML)	H <sub>2</sub> O (ML)	H <sub>2</sub> O <sub>2</sub> (ML)	O <sub>budget</sub> (ML)	O <sub>3</sub> (ML)	D <sub>2</sub> O (ML)	D <sub>2</sub> O <sub>2</sub> (ML)	O <sub>budget</sub> (ML)
$2/1 \times 10^{13}$	25	0.8	1.5	4.9	8.9	1.5	1.0	2.7	1.9
	40	2.7	1.8	2.3	-1.7	3.0	1.1	0.6	-6.7
	50	7.4	1.2	0.7	-19.6	8.8	1.8	0.5	-23.6
$8/4 \times 10^{13}$	25	0.8	3.1	4.6	9.9	1.5	1.6	2.2	1.5
	40	2.9	2.9	2.6	-0.6	2.7	1.6	1.4	-3.7
	50	8.1	3.7	1.8	-17.0	8.5	2.2	0.5	-22.3

### C. Possible reaction pathways

The investigation of the mass balance between the formed and consumed species in our ice after H/D-atom addition allows identifying the most likely reaction channel responsible for the formation of solid H<sub>2</sub>O ice. The mass balance for oxygen atoms can be determined looking at the number of O atoms present in each species (O<sub>budget</sub> = -3O<sub>3</sub> + H<sub>2</sub>O + 2H<sub>2</sub>O<sub>2</sub>). From the comparison of the results listed in Table II, we summarize three relevant results: (i) the O atoms are found in excess only at 25 K (O<sub>budget</sub> = 9.9/8.9 ML for higher/lower H-atom flux and 1.5/1.9 ML for both higher/lower D-atom flux); (ii) part of the O use-up is not converted into H<sub>2</sub>O/D<sub>2</sub>O and H<sub>2</sub>O<sub>2</sub>/D<sub>2</sub>O<sub>2</sub> at 40 and 50 K (negative O<sub>budget</sub>); and (iii) there appears to be a strong isotope effect in the formation of H<sub>2</sub>O/D<sub>2</sub>O and H<sub>2</sub>O<sub>2</sub>/D<sub>2</sub>O<sub>2</sub> (more H<sub>2</sub>O and H<sub>2</sub>O<sub>2</sub> than D<sub>2</sub>O and D<sub>2</sub>O<sub>2</sub>).

Point (i) can be explained by the presence of an extra O<sub>2</sub> poisoning layer deposited on top of the O<sub>3</sub> ice at 25 K. The extra O<sub>2</sub> originates from background deposition, while the substrate was cooled from 40 to 25 K with a rate of 1 K min<sup>-1</sup>. This effect is already minimized by lowering the surface temperature only after the main chamber pressure has substantially dropped toward the standard value of 10<sup>-10</sup> mbar. However, the deposition of a maximum of 5 ML of O<sub>2</sub> on top of the O<sub>3</sub> ice cannot be prevented for the 25 K experiments

(5 ML of O<sub>2</sub> correspond to 10 ML of O atoms). The higher value for the O<sub>budget</sub> in the 25 K hydrogenation experiment with respect to the deuteration experiment is consistent with a higher penetration depth of H atoms in the O<sub>2</sub> ice compared to D atoms.<sup>5</sup>

Point (ii) is addressed by the fact that most of the O<sub>2</sub> produced through reaction (1) is lost at temperatures higher than the O<sub>2</sub> ice desorption temperature. OH/OD and H<sub>2</sub>O/D<sub>2</sub>O can desorb upon reaction as well. We will discuss this issue in more detail in the next paragraph, which deals with point (iii).

Roughly the same amount of O<sub>3</sub> is used-up for the hydrogenation and deuteration experiments. This indicates that the observed isotope effect [point (iii)] is not due to a different rate for hydrogenation and deuteration of O<sub>3</sub>, but that it is probably caused by a different desorption probability upon reaction. Table II suggests that D<sub>2</sub>O and D<sub>2</sub>O<sub>2</sub> are more likely to desorb than H<sub>2</sub>O and H<sub>2</sub>O<sub>2</sub>. Thermal desorption, however, would lead to the reverse and therefore this effect has to come from the reaction energetics. We will first consider H<sub>2</sub>O/D<sub>2</sub>O, which is formed in two steps. In the first step, reaction (1), most of the excess energy will be released in the form of ro-vibrational excitation of OH/OD or in translational energy. Gas phase calculations show that this translational energy is 5.4% higher for deuteration than for hydrogenation,<sup>36</sup> which would lead to a slightly higher desorption probability for D + O<sub>3</sub> than for H + O<sub>3</sub> and may explain at least part of the observed effect. If H<sub>2</sub>O/D<sub>2</sub>O is then mainly formed from OH/OD through reaction (2) (see left side of Fig. 5), the large overall difference in desorption probability still cannot be fully explained. It can however be explained if H<sub>2</sub>O/D<sub>2</sub>O is mainly formed through reaction (3). In order to conserve momentum, the kinetic energy is distributed over the products according to the inverse mass. This means that D<sub>2</sub>O will have nearly twice the kinetic energy of H<sub>2</sub>O after reaction (3) ( $E_{D_2O}/E_D = 2/20$  and  $E_{H_2O}/E_H = 1/18$ ). Since the total excess energy of ~1 eV is close to the desorption energy of H<sub>2</sub>O (0.9 eV, Ref. 37), this difference in kinetic energy will have a substantial effect on the desorption probability. Therefore, in this case more D<sub>2</sub>O will desorb from the ice.

The observed isotope effect for H<sub>2</sub>O/D<sub>2</sub>O can thus be explained by reaction (3) instead of reaction (2). On first glance one would however expect reaction (2) to be more efficient than reaction (3), since the first is barrierless with an excess

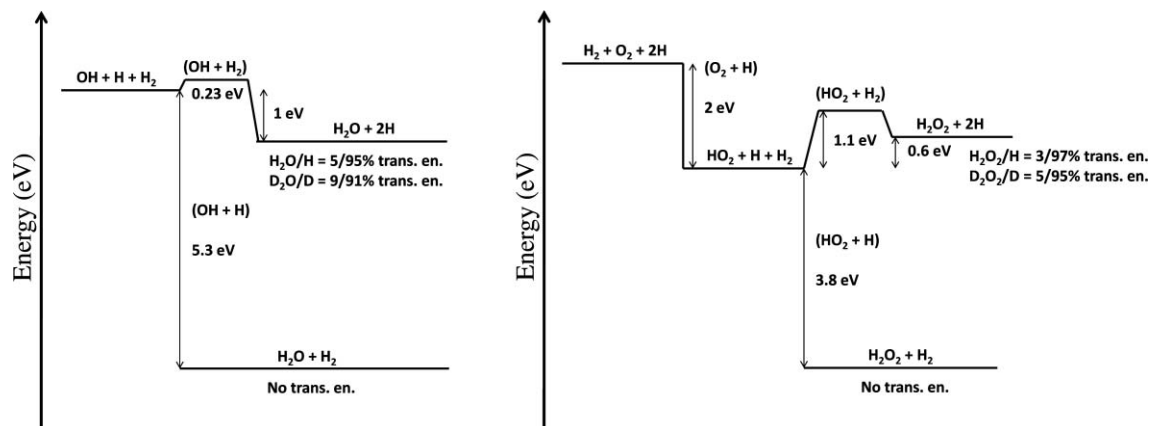


FIG. 5. Proposed reaction mechanism for the formation of H<sub>2</sub>O (left side) and H<sub>2</sub>O<sub>2</sub> (right side) from hydrogenation of O<sub>3</sub> ice. Reactions are shown in brackets.

of 5.3 eV, and the second has a barrier of 0.234 eV (Ref. 38) with an excess of 1 eV. The problem with reaction (2) is that one needs to dissipate 5.3 eV of excess energy with just one product. Part of this could be absorbed by the ice surface, but the weak interactions between the product and the ice limits the full dissipation. A reaction where only 1 eV of excess energy is released over two products is therefore more likely, especially since H<sub>2</sub> is abundantly present in our experiment, because the H-atom beam entering the main chamber contains a large fraction of cold H<sub>2</sub>.

Furthermore, gas phase experiments indicate that tunneling becomes important for OH + H<sub>2</sub> below 250 K. The reaction rate at 25–50 K will therefore be substantially increased through tunneling. This also leads to an extra isotope effect where OH + H<sub>2</sub> has probably a higher rate than D<sub>2</sub> + OD. In addition, OH/OD is formed “hot” and this energy can also be used to overcome the reaction barrier. Reaction (3) may therefore be more relevant than reaction (2). These two reactions were previously included in the complete reaction network for O<sub>2</sub> surface hydrogenation investigated in Ref. 9, although no experimental evidence was found for reaction (3). However, the method used there was not very sensitive to the detection of this particular reaction. Therefore, extra dedicated studies specifically on the OH + H<sub>2</sub> reaction are needed to determine the absolute efficiency of this reaction, especially in light of the present study, which indicates that this reaction may be crucial as a final step in all three water formation channels (O/O<sub>2</sub>/O<sub>3</sub> + H).

Similar arguments can be used for the formation of H<sub>2</sub>O<sub>2</sub>/D<sub>2</sub>O<sub>2</sub> from HO<sub>2</sub>/DO<sub>2</sub> by



or



where the latter can again lead to an isotope effect with more D<sub>2</sub>O<sub>2</sub> than H<sub>2</sub>O<sub>2</sub> desorption and a lower rate of reaction for D<sub>2</sub> + DO<sub>2</sub> through tunneling (see right side of Fig. 5). HO<sub>2</sub> + H<sub>2</sub> has a high barrier of 1.1 eV and is endothermic by –0.6 eV. However, in the aforementioned study we have observed this reaction to proceed.<sup>9</sup> The exothermicity of O<sub>2</sub> + H may help to overcome the barrier and the endothermicity, since the total reaction



composed of



and



is exothermic by 1.3 eV.

To summarize, the observed isotope effect between H<sub>2</sub>O/H<sub>2</sub>O<sub>2</sub> and D<sub>2</sub>O/D<sub>2</sub>O<sub>2</sub> in the O<sub>3</sub> hydrogenation channel can be explained by a combination of effects. First, OD will get more translational energy than OH in reaction (1). Then, if H<sub>2</sub>O<sub>2</sub> and H<sub>2</sub>O are formed through reactions with H<sub>2</sub>, tunneling leads to a higher rate for hydrogenation than deuteration, and second, the distribution of excess energy can

lead to more D<sub>2</sub>O/D<sub>2</sub>O<sub>2</sub> than H<sub>2</sub>O/H<sub>2</sub>O<sub>2</sub> desorption. O<sub>3</sub> is destroyed equally for H and D, which indicates that reaction (1) proceeds without substantial tunneling effect.

Finally, all the experimental results discussed here, i.e., points (i), (ii), and (iii), are obtained under laboratory conditions, and consequently some parameters necessarily differ orders of magnitude from those typical for interstellar conditions, i.e., the time scale to reach a comparable H-atom fluence. More critically, the use of excess energy to allow further reaction steps in the laboratory may be absent under astronomical conditions. The excess energy of the OH radical formed through reaction (1), for example, may be dissipated in the ice before H<sub>2</sub> would reach this radical on an interstellar timescale. However, a two step reaction mechanism may still apply to the interstellar medium at low temperature (10 K), if an H<sub>2</sub> layer is available on the surface of the ice for further reactions. However, the differences between laboratory and interstellar conditions do not change the main conclusion of the work presented here: water is formed efficiently at low temperatures through hydrogenation of O<sub>3</sub> ice and reaction (3) may be more relevant than reaction (2) under interstellar ice analog conditions.

## V. CONCLUSION

The present study shows that the water formation through hydrogenation of solid O<sub>3</sub> ice as proposed by Tielens and Hagen<sup>1</sup> takes place under interstellar ice analog conditions. Hydrogenation of O<sub>3</sub> ice exhibits a similar temperature dependency as seen for CO ice:<sup>24</sup> the mobility of O<sub>3</sub> molecules increases with the temperature, while the penetration depth of H atoms into the ice involves only the first monolayers. For temperatures above the O<sub>2</sub> desorption temperature, hydrogenation of O<sub>3</sub> leads to erosion of the ice, since O<sub>2</sub> formed in the reaction O<sub>3</sub> + H desorbs. The remaining OH can further react to H<sub>2</sub>O and H<sub>2</sub>O<sub>2</sub>. The erosion occurs until a layer of H<sub>2</sub>O and H<sub>2</sub>O<sub>2</sub> layer covers the ice and prevents the incoming H atoms from reaching the underlying O<sub>3</sub> ice. It is found that at high surface temperature (50 K) O<sub>3</sub> is mobile enough to slowly diffuse through the H<sub>2</sub>O and H<sub>2</sub>O<sub>2</sub> layer and to become available for further hydrogenation on the surface of the ice.

Experimental evidence is found for the connection of the O<sub>3</sub> hydrogenation channel to the O + H and O<sub>2</sub> + H channels, as summarized in Fig. 1. As a result it has become possible to draw conclusions on several reactions that are part of the other two hydrogenation channels. The results indicate that the reaction OH + H<sub>2</sub> is most likely more efficient than the reaction OH + H: reaction OH + H<sub>2</sub> could proceed through tunneling, while reaction OH + H needs to dissipate 5.3 eV of excess energy with just one product, which could be difficult. Our experimental results complete the reaction scheme initially proposed in Ref. 1 to explain surface water formation in space. The conclusion that the three channels (O/O<sub>2</sub>/O<sub>3</sub> + H) are strongly linked is of importance for astrochemical models focusing on water formation under interstellar conditions.

## ACKNOWLEDGMENTS

We thank M. van Hemert, T. P. M. Goumans, C. Arasa, E. Fayolle and K. I. Öberg for stimulating and fruitful discussions, and G. Schwaab (University of Bochum) for providing the ozone generator. The research leading to these results has received funding from NOVA, the Netherlands Research School for Astronomy, a Spinoza grant from the Netherlands Organization for Scientific Research, NWO, and the European Community's Seventh Framework Programme (FP7/2007-2013) under Grant Agreement No. 238258.

- <sup>1</sup>A. G. G. M. Tielens and W. Hagen, *Astron. Astrophys.* **114**, 245 (1982).
- <sup>2</sup>K. Hiraoka, T. Miyagoshi, T. Takayama, K. Yamamoto, and Y. Kihara, *Astrophys. J.* **498**, 710 (1998).
- <sup>3</sup>F. Dulieu, L. Amiaud, E. Congiu, J. Fillion, E. Matar, A. Momeni, V. Pirronello, and J. L. Lemaire, *Astron. Astrophys.* **512**, A30 (2010).
- <sup>4</sup>N. Miyauchi, H. Hidaka, T. Chigai, A. Nagaoka, N. Watanabe, and A. Kouchi, *Chem. Phys. Lett.* **456**, 27 (2008).
- <sup>5</sup>S. Ioppolo, H. M. Cuppen, C. Romanzin, E. F. van Dishoeck, and H. Linnartz, *Astrophys. J.* **686**, 1474 (2008).
- <sup>6</sup>E. Matar, E. Congiu, F. Dulieu, A. Momeni, and J. L. Lemaire, *Astron. Astrophys.* **492**, L17 (2008).
- <sup>7</sup>Y. Oba, N. Miyauchi, H. Hidaka, T. Chigai, N. Watanabe, and A. Kouchi, *Astrophys. J.* **701**, 464 (2009).
- <sup>8</sup>S. Ioppolo, H. M. Cuppen, C. Romanzin, E. F. van Dishoeck, and H. Linnartz, *Phys. Chem. Chem. Phys.* **12**, 12065 (2010).
- <sup>9</sup>H. M. Cuppen, S. Ioppolo, C. Romanzin, and H. Linnartz, *Phys. Chem. Chem. Phys.* **12**, 12077 (2010).
- <sup>10</sup>H. Mokrane, H. Chaabouni, M. Accolla, E. Congiu, F. Dulieu, M. Chehrouri, and J. L. Lemaire, *Astrophys. J. Lett.* **705**, L195 (2009).
- <sup>11</sup>M. Famá, D. A. Bahr, B. D. Teolis, and R. A. Baragiola, *Nucl. Instrum. Methods Phys. Res. B* **193**, 775 (2002).
- <sup>12</sup>M. J. Loeffler, U. Raut, R. A. Vidal, R. A. Baragiola, and R. W. Carlson, *Icarus* **180**, 265 (2006).
- <sup>13</sup>P. D. Cooper, M. H. Moore, and R. L. Hudson, *Icarus* **194**, 379 (2008).
- <sup>14</sup>L. Schriver-Mazzuoli, A. de Saxcé, C. Lugez, C. Camy-Peyret, and A. Schriver, *J. Chem. Phys.* **102**, 690 (1995).
- <sup>15</sup>P. A. Gerakines, W. A. Schutte, and P. Ehrenfreund, *Astron. Astrophys.* **312**, 289 (1996).
- <sup>16</sup>S. Lacombe, F. Cemic, K. Jacobi, M. N. Hedhili, Y. Le Coat, R. Azria, and M. Tronc, *Phys. Rev. Lett.* **79**, 1146 (1997).
- <sup>17</sup>C. J. Bennett and R. I. Kaiser, *Astrophys. J.* **635**, 1362 (2005).
- <sup>18</sup>B. Sivaraman, C. S. Jamieson, N. J. Mason, and R. I. Kaiser, *Astrophys. J.* **669**, 1414 (2007).
- <sup>19</sup>K. S. Noll, R. E. Johnson, A. L. Lane, D. L. Domingue, and H. A. Weaver, *Science* **273**, 341 (1996).
- <sup>20</sup>K. S. Noll, T. L. Roush, D. P. Cruikshank, R. E. Johnson, and Y. J. Pendleton, *Nature (London)* **388**, 45 (1997).
- <sup>21</sup>A. R. Hendrix, C. A. Barth, and C. W. Hord, *J. Geophys. Res.* **104**, 14169 (1999).
- <sup>22</sup>H. M. Cuppen and E. Herbst, *Astrophys. J.* **668**, 294 (2007).
- <sup>23</sup>S. Cazaux, V. Cobut, M. Marseille, M. Spaans, and P. Caselli, *Astron. Astrophys.* **522**, A74 (2010).
- <sup>24</sup>G. W. Fuchs, H. M. Cuppen, S. Ioppolo, S. E. Bisschop, S. Andersson, E. F. van Dishoeck, and H. Linnartz, *Astron. Astrophys.* **505**, 629 (2009).
- <sup>25</sup>D. D. Berkley, B. R. Johnson, N. Anand, K. M. Beauchamp, and L. E. Conroy, *Appl. Phys. Lett.* **53**, 1973 (1988).
- <sup>26</sup>K. Acharyya, G. W. Fuchs, H. J. Fraser, E. F. van Dishoeck, and H. Linnartz, *Astron. Astrophys.* **466**, 1005 (2007).
- <sup>27</sup>H. Chaabouni, L. Schriver-Mazzuoli, and A. Schriver, *Low Temp. Phys.* **26**, 712 (2000).
- <sup>28</sup>E. Y. Misochko, A. V. Akimov, and C. A. Wight, *J. Phys. Chem. A* **103**, 7972 (1999).
- <sup>29</sup>K. G. Tschersich and V. von Bonin, *J. Appl. Phys.* **84**, 4065 (1998).
- <sup>30</sup>K. G. Tschersich, *J. Appl. Phys.* **87**, 2565 (2000).
- <sup>31</sup>K. G. Tschersich, J. P. Fleischhauer, and H. Schuler, *J. Appl. Phys.* **104**, 034908 (2008).
- <sup>32</sup>P. A. Giguère and K. B. Harvey, *J. Mol. Spectrosc.* **3**, 36 (1959).
- <sup>33</sup>D. F. Hornig, H. F. White, and F. P. Reding, *Spectrochim. Acta* **12**, 338 (1958).
- <sup>34</sup>J. A. Lannon, F. D. Verderame, and R. W. Anderson, Jr., *J. Chem. Phys.* **54**, 2212 (1971).
- <sup>35</sup>P. Brosset, R. Dahoo, B. Gauthierroy, L. Abouafmarguin, and A. Lakhlifi, *Chem. Phys.* **172**, 315 (1993).
- <sup>36</sup>H. G. Yu and A. J. C. Varandas, *J. Chem. Soc., Faraday Trans.* **93**, 2651 (1997).
- <sup>37</sup>S. Andersson, A. Al-Halabi, G. Kroes, and E. F. van Dishoeck, *J. Chem. Phys.* **124**, 064715 (2006).
- <sup>38</sup>M. Yang, D. H. Zhang, M. A. Collins, and S. Lee, *J. Chem. Phys.* **115**, 174 (2001).